Higher-order resonant modes in a photonic heterostructure nanocavity

Yasushi Takahashi,[a] Yoshinori Tanaka, Hiroyuki Hagino, Takashi Asano, and
Susumu Noda

*Department of Electronic Science and Engineering and Photonics and Electronics Science and Engineering
Center, Kyoto University, Kyoto 615-8510, Japan*

We investigated the optical characteristics of higher-order resonant modes for a heterostructure nanocavity formed in a two-dimensional photonic-crystal silicon slab. Two kinds of resonant modes were observed, the nanocavity modes and the Fabry–Pérot modes. High quality factors of more than 1.0×10^6 were obtained not only for the nanocavity mode but also for the Fabry–Pérot modes. © *2008 American Institute of Physics*. [DOI: 10.1063/1.2943650]

Two-dimensional (2D) photonic-crystal (PC) nanocavities are drawing much attention due to their high quality factors (Q) and small modal volumes of almost one cubic wavelength in the material.[1–4] Recently, we have succeeded in increasing Q values of 2D-PC nanocavities using the photonic heterostructure.[5,6] This structure is highly flexible and is able to achieve a theoretical Q value (Q_{ideal}) over 10^6 up to 10^9 in various ways while retaining a small modal volume.[7–9] Therefore, heterostructure nanocavities show great promise for both practical applications and studies of fundamental physical phenomena.[10,11]

Because the highest Q_{ideal} in a heterostructure nanocavity is generally obtained in the fundamental resonant mode, research has so far focused on the fundamental mode with little attention paid to higher-order resonant modes. Recently, it was found that higher-order modes were useful for highly efficient selective excitation of light emitters embedded in several types of nanocavities.[11,12] It was also suggested that they might be very useful for obtaining enhancement of spontaneous emission or Raman lasing in silicon (Si) nanocavities.[13,14] Therefore, there is an emerging interest in the higher-order modes of the heterostructure nanocavities.

In this paper, we report on the characteristics of the higher-order modes in a two-step heterostructure nanocavity formed in a 2D-PC Si slab. It is shown that two kinds of resonant modes exist: the nanocavity modes and the Fabry–Pérot (FP) modes. We investigate the Q, frequencies, emission patterns, and the polarizations for these modes. Experimental Q factors are found to exceed 1.0×10^6 not only for the nanocavity mode but also for the FP modes.

Figure 1(a) shows a scanning electron microscope (SEM) image of the device studied in this work, which was fabricated using the same procedure as previously reported.[5] The 2D-PC consists of a triangular lattice of circular air holes with radii of 120 nm formed in a 250-nm-thick Si slab. Two line defects are fabricated in parallel. The lower one, which is regarded as a FP cavity with 39 missing holes, is a required component of the heterostructure nanocavity. The nanocavity with a two-step heterostructure is formed at the center of the FP cavity, in which the lattice constant in the x direction increases as it approaches the center as shown in Fig. 1(b). These values of the central (PC2), intermediate (PC2′), and outer regions (PC1) of the nanocavity are a_2

$=420$ nm, $a_2'=415$ nm, and $a_1=410$ nm, respectively, while the lengths are $2a_2$, $2a_2'$, and $17a_1$, respectively (the lattice constant in the y direction are the same for all regions). As a result, the lower line defect's band structure is formed, as pictured in Fig. 1(c), where two types of resonant modes are consequently produced: nanocavity modes for frequencies below the edge of the transmission band in PC1 (dotted curve) and FP modes above the PC1 band edge (solid curve). It is noted that the former are locally confined in the center region (PC2 and PC2′) due to the mode gap differences while the latter are spread out in all three regions. Thus, FP modes inevitably exist at the higher frequency side in the general heterostructure nanocavities. The upper, wider line defect in Fig. 1(a) is the excitation waveguide used to inject light into the cavity via evanescent mode coupling. The distance between the two line defects was set to four rows of air holes for sufficient coupling of all resonant modes.

We performed the microscopic-transmission measurement for the device in Fig. 1(a) at room temperature. The
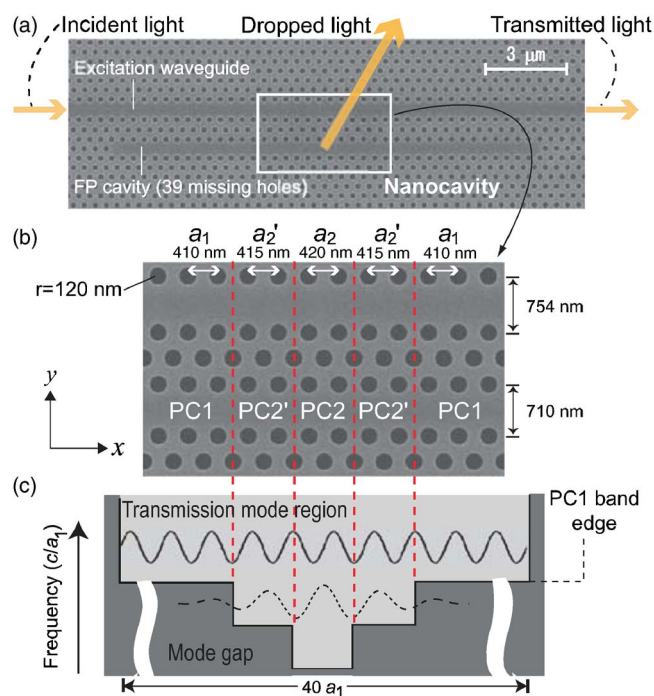

FIG. 1. (Color online) (a) SEM topview around the cavity. (b) Magnified view at the nanocavity. (c) Schematic band structure for the FP cavity. The dotted (solid) curve represents the nanocavity (FP) mode.
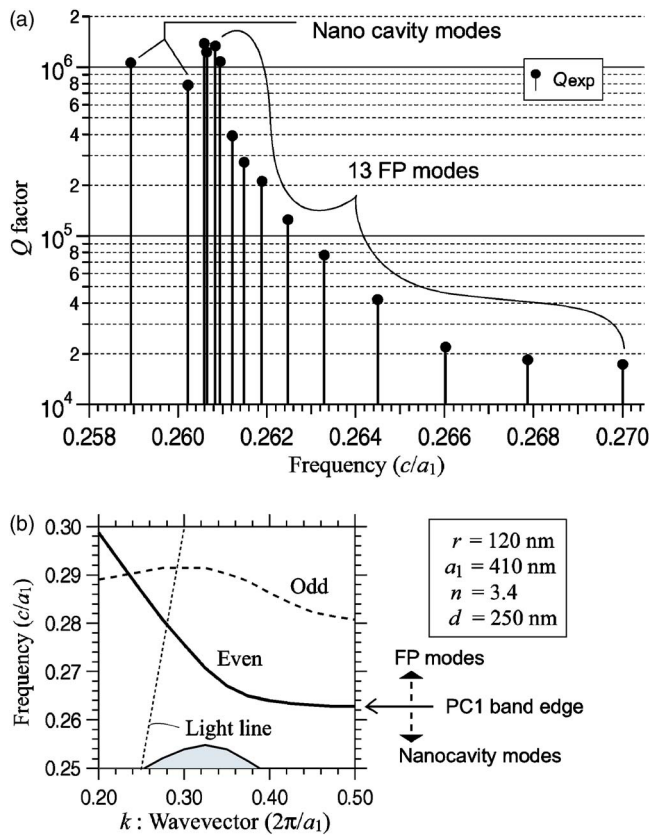
a)Electronic mail: ytakahashi@qoe.kuee.kyoto-u.ac.jp.

FIG. 2. (Color online) (a) Frequencies and Q_{exp} for 15 resonant modes. (b) Band diagram of the line-defect waveguide in PC1. Parameters used in calculation are inserted.

configuration of incident, dropped, and transmitted light is illustrated in Fig. 1(a), where the light source was a tunable-wavelength continuous-wave semiconductor laser. The dropped light from the cavity to the vertical direction could be observed provided the incident wavelength matched the resonant wavelength. We measured the spectra for the dropped light and for the transmitted light through the excitation waveguide, and measured near field images and polarization properties for the dropped light. In order to obtain intrinsic Q factors (Q_{exp}) of the resonant modes, the effect of the loading due to the excitation waveguide was excluded using both spectra. The details of the experiment and the estimation of Q_{exp} are described in other papers.[6,15]

The graph in Fig. 2(a) presents the frequencies and Q_{exp} for the 15 resonant modes observed between 1515 and 1585 nm. In order to distinguish the nanocavity modes from the FP modes, we fabricated a reference sample on the same chip, close to the device shown in Fig. 1(a). The structure of the reference is the same as Fig. 1(a), except that PC2 and PC2′ are replaced with PC1 so that the nanocavity modes are not observed. The two lowest-energy modes in Fig. 2(a) were not observed in the reference sample, while the other 13 modes above $f=0.2606$ were observed at similar frequencies with similar Q_{exp}. Therefore, we can classify the 15 resonant modes as 2 nanocavity modes and 13 FP modes. We can also determine the PC1 band edge to be at $f=0.2606$. For comparison, we calculated the mode dispersion curve of the line defect in PC1 region by the three-dimensional (3D) finite-difference time-domain (FDTD) method, as shown in Fig. 2(b), where the even mode is the mode utilized for the nano-

cavity. It is found that the PC1 band edge is very close to the experimental result.

The mode at $f=0.2589$ with Q_{exp} of 1.1×10^6 is the fundamental nanocavity mode that we have reported in previous papers,[5,6] whose Q_{ideal} and modal volume are 1.2×10^7 and $1.3(\lambda/n)^3$ according to 3D FDTD. The mismatch between Q_{exp} and Q_{ideal} is due to structural imperfections in the fabricated cavity,[15] which give rise to an additional Q factor (Q_{loss}). According to the relationship $1/Q_{exp}=1/Q_{ideal}+1/Q_{loss}$, Q_{loss} for this mode is 1.2×10^6. The mode at $f=0.2602$ is the second-order nanocavity mode, whose Q_{exp} is also as high as 8.0×10^5. Assuming the same Q_{loss} of 1.2×10^6, Q_{ideal} for the second mode is estimated to be 2.4×10^6. It is noted that we can control the Q_{ideal} and frequencies of higher-order nanocavity modes to some extent by changing the design of the heterostructure. These modes might be useful for the study of a coupled system in which two nanocavity modes are simultaneously resonant with two types of excitonic states of a emitter.

The frequencies of the FP modes can be evaluated from the dispersion curve shown in Fig. 2(b) and the FP resonance condition of $k=(\pi/L)\mathbf{m}$, where k is the wavevector, L is the cavity length, and $\mathbf{m}$ is the modal integer number. By letting L be $40a_1$, it is calculated that FP modes are formed every wavevector interval of $\delta k=2\pi/80a_1$. It is found from Fig. 2(b) that the observed frequency range for FP modes ($f=0.2606–0.2700$) correspond to the wavevector range $k\cong0.33–0.5$ in the dispersion curve. By dividing the width of the wavevector range by δk, the expected number of FP modes in the observed frequency range is calculated to be $0.17/(1/80)=13.6$. It is also expected from the slope of the dispersion curve that frequency intervals are smaller near the PC1 band edge and larger at the higher frequency side. The experimental results are in good agreement with these theoretical predictions.

The Q_{exp} of first to fourth FP modes ($\mathbf{m}=1–4$) are as large as 1.0×10^6. However, the Q_{ideal} for these modes are actually much larger than 1.0×10^6,[16] which means that Q_{exp} for these modes are also restricted by a Q_{loss} of about 1.3×10^6. Similar values of Q_{loss} for the nanocavity and FP modes suggests that the main causes of Q_{loss} in both cases may be the same. Therefore, improvements for decreasing the structural imperfections are very important to increase the Q_{exp} in both kinds of modes.

The Q_{exp} from the 4th to the 13th FP mode decreases monotonically. This implies that Q_{ideal} is smaller for higher-order modes. In order to verify this, we simulated a FP cavity with nine missing air holes, as shown in Fig. 3(a), by 3D FDTD, where the same structural parameters as in Fig. 2(b) were used. In this calculation, four resonant modes of first to the fourth were found at frequencies of 0.2631, 0.2649, 0.2686, and 0.2765. Q_{ideal} for these modes were 3.3×10^5, 5.0×10^4, 8.6×10^3, and 2.5×10^3, respectively. The frequency intervals and monotonic reduction of Q_{ideal} coincide well with the experiment's characteristics (the difference in the absolute value of Q_{ideal} between the simulation and the experiment can be explained by the difference in the cavity length). The decrease of Q_{ideal} for higher-order mode can be explained in the same manner as reported for the high-Q nanocavities. In 2003, we reported that the out-of-slab radiation leakage from the nanocavities is mainly caused by the abrupt change of the electric field at the cavity edges.[1] It was
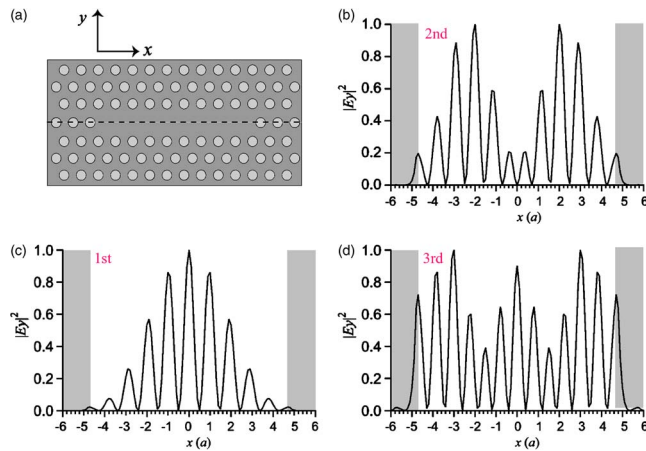
FIG. 3. (Color online) (a) Illustration of FP cavity with nine missing air holes. [(b)–(d)] The profile of $|E_y|^2$ for the first to third FP modes along the dotted line in (a). Shaded parts indicate the cavity edges.

demonstrated that the ideal envelope function of the electric field for nanocavity mode is a Gaussian function, because smooth decay and localization of the field is simultaneously obtained. Figures 3(b)–3(d) show the profile of the electric-field squared, $|E_y|^2$, for the first to third modes along the dotted line in Fig. 3(a). The profile of $|E_y|^2$ tends to spread out and have a more abrupt change at the edges as the mode order increases. This is because the shape of the envelope functions of $|E_y|^2$ can be approximately expressed by $\sin^2(\mathbf{m}\pi/L)(x+L/2)$, which is similar to that of an electron confined in a quantum well. We think that this feature might be the cause of the monotonic decrease of Q_{ideal} for higher-order FP modes.

Figure 4 shows the experimental near field images and polarization properties of dropped light for the first nanocavity mode, and the first, second, and ninth FP modes. White dashed lines superimposed on each image indicate the position of the line defects. The spatial resolution of the image is about 2 μm. The image for $f=0.2589$ confirms that it is a nanocavity mode because the emission is located at the center of the heterostructure. We confirmed a similar characteristic for second nanocavity mode at $f=0.2602$. The emission pattern for the ninth FP mode shows that the radiation leakage mainly occurs at the FP cavity edges, which agrees with the aforementioned leakage mechanism. This property was consistently retained between the 5th and 13th FP modes.
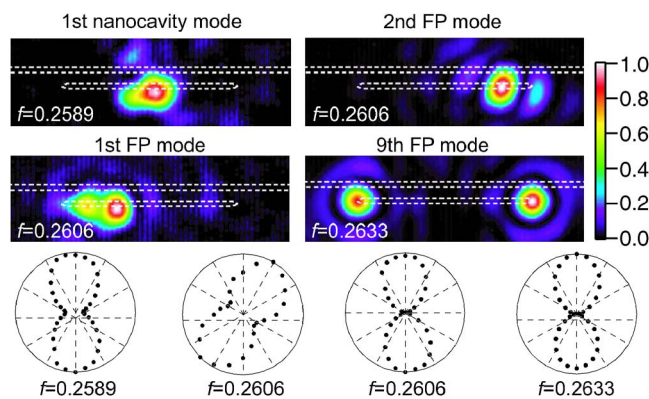

FIG. 4. (Color online) Near field images and polarization properties for four resonant modes. Corresponding frequencies and line defects structure are superimposed.

However, the radiation leakage for the modes with Q_{exp} greater than 1.0×10^6 is due to the Q_{loss}, and therefore, the emission for the first and second FP modes are not located at the edges. Because the structural imperfections are randomly introduced into the cavity during fabrication, the positions of dropped light could be random for such modes.

The dropped light from the resonant modes originating from the even dispersion curve should polarize in the y direction because the polarized light in the x direction tends to disappear due to the far-field cancellation effect.[16] This polarization selection rule was confirmed in the experiment shown in Fig. 4. However, it is not always conserved in the modes for which Q_{ideal} is larger than Q_{loss}, for instance in the case of the first FP mode.

It is noted that the number of FP modes and its frequencies depend on the length of a FP cavity. It has been confirmed that we can decrease the length of a FP cavity to $\sim$5 μm (11 or 13 missing air holes) while maintaining Q_{ideal} for the fundamental nanocavity mode over 1.0×10^7. We think that the FP modes would be useful for selective excitation of nanocavity emitters and Raman lasing in collaboration with the nanocavity modes.

In summary, we have investigated the higher-order resonant modes of a heterostructure nanocavity formed in a 2D-PC Si slab, and both the nanocavity modes and the FP modes have been observed. The coexistence of two types of cavity modes is intrinsic feature for heterostructure cavities. The Q_{exp} more than 1.0×10^6 have been obtained not only for the nanocavity mode but also for some FP modes.

[1]Y. Akahane, T. Asano, B. S. Song, and S. Noda, Nature (London) **425**, 944 (2003).

[2]M. Nomura, S. Iwamoto, K. Watanabe, N. Kumagai, Y. Nakata, S. Ishida, and Y. Arakawa, Opt. Express **14**, 6308 (2006).

[3]K. Hennessy, A. Badolato, M. Winger, D. Gerace, M. Atature, S. Gulde, S. Falt, E. L. Hu, and A. Imamoglu, Nature (London) **445**, 896 (2007).

[4]Y. Tanaka, J. Upham, T. Nagashima, T. Sugiya, T. Asano, and S. Noda, Nat. Mater. **6**, 862 (2007).

[5]B. S. Song, S. Noda, T. Asano, and Y. Akahane, Nat. Mater. **4**, 207 (2005).

[6]Y. Takahashi, H. Hagino, Y. Tanaka, B. S. Song, T. Asano, and S. Noda, Opt. Express **15**, 17206 (2007).

[7]S. Tomljenovic-Hanic, C. M. Sterke, and M. J. Steel, Opt. Express **14**, 12451 (2006); S. Tomljenovic-Hanic, M. J. Steel, C. M. Sterke, and D. J. Moss, Opt. Lett. **32**, 542 (2007).

[8]S. H. Kwon, T. Sunner, M. Kamp, and A. Forchel, Opt. Express **16**, 4605 (2008).

[9]Y. Tanaka, T. Asano, and S. Noda, J. Lightwave Technol. **26**, 1532 (2008).

[10]T. Yang, A. Mock, J. O'brien, S. Lipson, and D. G. Deppe, Opt. Lett. **32**, 1153 (2007).

[11]W. C. Stumpf, M. Fujita, M. Yamaguchi, T. Asano, and S. Noda, Appl. Phys. Lett. **90**, 231101 (2007).

[12]M. Nomura, S. Iwamoto, M. Nishioka, S. Ishida, and Y. Arakawa, Appl. Phys. Lett. **89**, 161111 (2006); M. Nomura, S. Iwamoto, T. Yang, S. Ishida, and Y. Arakawa, *ibid.* **89**, 241124 (2006).

[13]S. Iwamoto, Y. Arakawa, and A. Gomyo, Appl. Phys. Lett. **91**, 211104 (2007).

[14]X. Yang and C. W. Wong, Opt. Express **13**, 4723 (2005); **15**, 4763 (2007).

[15]T. Asano, B. S. Song, and S. Noda, Opt. Express **14**, 1996 (2006).

[16]S. H. Kim, G. H. Kim, S. K. Kim, H. G. Park, and Y. H. Lee, J. Appl. Phys. **95**, 411 (2004).